On the Potential of Orbital VHF Sounding Radars to Locate Shallow Aquifers in Arid Areas Using Reflectometry

Sanchari Thakur, Essam Heggy, *Member, IEEE*, Mark S. Haynes, *Member, IEEE*, Elizabeth M. Palmer, and Lorenzo Bruzzone, *Fellow, IEEE*

Abstract— Shallow aquifers are the primary water source to mitigate rising hydroclimatic fluctuations in arid areas, notably in North Africa and the Arabian Peninsula. The occurrence and dynamics of these expansive water bodies remain poorly characterized due to the reliance on sporadic monitoring wells. To address this deficiency, several studies are exploring the potential of low Earth orbit sounding radars as a large-scale mapping tool that can provide unique insights into the delineation and dynamics of these aquifers. Herein, we analyze the detectability of shallow aquifers (<10 m deep) using the radiometric analysis of surface reflections from a 45-MHz orbital sounder with an 8-MHz bandwidth. We use the ray tracing method to simulate the radar return from two realistic geoelectrical and topographic models of shallow aquifers in North African Sahara desert for omnidirectional and distributed array configurations. Our results suggest that the dielectric change induced by shallow aquifers that are up to 10-m deep can increase the 45-MHz radar surface return of the desiccated desert surface by 5 dB in areas with very low surface roughness of rms height <0.35 m. These preliminary results suggest a constrained potential for a monostatic VHF reflectometry to probe large sedimentary basins, which a distributed architecture can improve.

Index Terms— Deserts, radar sounder, reflectometry, shallow aquifers.

I. INTRODUCTION

SOUNDING radars are nadir-looking low-frequency instruments, mostly from 1 to 100 MHz, which can profile the near-surface of Earth and planetary bodies. Earth-orbiting sounding radar missions have been recently proposed to map the polar ice-caps and warm, arid deserts to support forecasting sea level rise and freshwater resource assessment,

respectively [1]. Cold and warm deserts, which are mainly composed of ice and sand formations, are favorable environments for VHF radar wave penetration. While VHF-sounding radar investigations of the polar regions in Greenland and Antarctica have an extensive scientific and engineering heritage built over decades of airborne acquisitions, the potential for probing shallow aquifers remains largely unconstrained. To this day, the occurrence, delineation, and dynamics of these strategic water bodies, which are crucial in mitigating rising hydroclimatic fluctuations in arid areas, are primarily derived from sporadic well logs in the absence of large-scale mapping methods that can operate in these harsh environments. To address this deficiency, there have been a few airborne radar sounder campaigns in Morocco [2] and several others proposed in the Arabian Peninsula [3]. Furthermore, to mitigate the challenges in airborne acquisitions (nonhomogeneous data quality, nonuniform coverage, high cost), Earth-orbiting sounding radar missions have been proposed to support the detection of shallow aquifers. Several instrumental and geophysical factors, such as the surface clutter, the radar blind zone, and the variability in penetration depth across the expansive deserts of North Africa and the Arabian Peninsula, can compromise the direct detection of the water table in aquifer systems. As such, we propose herein to use surface reflectometry to infer the presence of shallow aquifers in the first 10 m.

Conventionally, radar sounders deploy omnidirectional dipole antennas, which produce a large antenna pattern. As a result, radar echoes from a large off-nadir surface area contribute to clutter that can mask the aquifer's response, compromising its detectability. The large antenna pattern also reduces across-track resolution. This limitation can be overcome by increasing the antenna length or using synthetic aperture methods. However, deploying a very large physical antenna is not feasible due to mechanical constraints. Recently, a novel radar sounder architecture has been proposed to allow the deployment of very large antennas using an array of small satellites in orbital flying formation [4]. The resulting very large across-track antenna aperture helps reduce the across-track clutter and improve the resolution, as well as improve the signal-to-noise ratio.

In this investigation, we consider a low Earth-orbiting radar sounder operating at a central frequency of 45 MHz with an 8-MHz bandwidth, which is the basis for the

proposed SaTellite RAdar sounder for Earth subsurface Sensing (STRATUS) [1] and Orbiting Arid Subsurface and Ice Sheet Sounder (OASIS) [5] missions. Previous studies [6], [7], [8] have shown the feasibility of a 45-MHz radar sounder with the conventional dipole antenna to observe the Earth from a satellite platform, overcoming the effects of ionosphere, clutter, and galactic noise. We specifically analyze the sensitivity of the 45-MHz sounder to the presence of shallow aquifers in arid deserts for two types of satellite configurations: 1) the conventional omnidirectional transmitting–receiving antenna and 2) the novel distributed architecture comprising five transmitting–receiving antennas deployed in the across-track direction. The analysis is based on simulating the radar response of parametric aquifer models using a coherent ray-tracing-based approach [9].

II. METHODOLOGY

A. Description of Aquifer Characteristics

As study areas, we have selected two basins in north-central Libya: 1) Ma'tan al Jafr, a well in Ajdabia (29.85°N, 19.7°E), and 2) Marada oasis in Al Wahat district (29.4°N, 19.22°E). These were selected because of their potential for groundwater mounding from deeper aquifers through the fault system in each basin. Laboratory measurements and field surveys indicate that the dielectric properties of desiccated desert materials range from $\epsilon' = 2 - 8$ and $\epsilon'' = 0.01 - 0.25$, where ϵ' is the real part of the permittivity while ϵ'' is the imaginary part [10], [11]. For shallow aquifers in the Sahara and Arabian deserts, the water table is typically <50 m deep [10], [12]. Shallow aquifers are located by definition in the flat, low-lying parts of basins, which are filled with smooth sedimentary deposits with root-mean-squared height (h_{rms}) less than 1 m within the radar footprint [11]. Analysis of well-logs data and literature shows that a significant portion of the water table in large aquifer systems occurs within the top 50 m of the surface.

B. Theoretical Background on VHF Orbital Reflectometry

Reflectometry techniques analyze the surface echo signal power to obtain information on the near-surface zone. This zone is defined by the antenna footprint (horizontal limit) and the radar range resolution in the medium (vertical limit). For orbital-sounding radars such as STRATUS or OASIS, shallow aquifers are naturally present in relatively flat areas within the near-surface (range resolution <10 m), enabling their detection by the state-of-the-art reflectometry techniques. In particular, the high dielectric contrast between water and dry sands is expected to enhance the echo strength, favoring the detectability. Fig. 1(a) shows the ratio of the reflectivity of an aquifer to that of the air–sand interface for a range of sand dielectric properties and water table depths. In the absence of surface roughness, assuming that the aquifer response dominates the surface echo, a difference of about 5 dB in surface power can indicate the presence of an aquifer.

Besides the geoelectrical properties of the investigated site, in reality the surface echo also depends on the roughness and the ionospheric characteristics during acquisition. Ionospheric
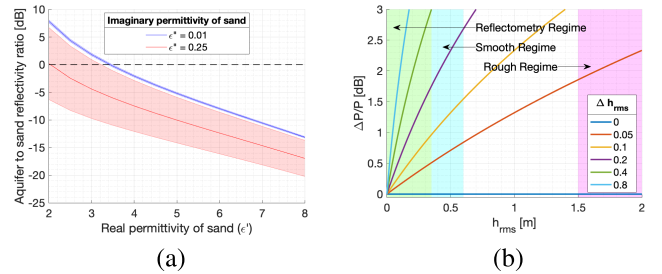

Fig. 1. (a) Fresnel reflectivity of aquifer to dry sand ratio plotted against the real permittivity of the sand layer, for different values of the imaginary permittivity. The envelopes represent the range of depths of the aquifer (1–10 m). (b) Relative uncertainty in linear power due to roughness versus h_{rms} for different values of uncertainty in the rms height. The ranges of h_{rms} values that are very smooth, smooth, and rough at radar wavelength are indicated in green, blue, and magenta, respectively.

delay and signal distortion are minimal during night acquisition for North Africa and the Arabian Peninsula [13]. The variation in surface echo power P due to roughness, described by h_{rms}, is given by

$$P = e^{-(2kh_{rms})^2} \qquad (1)$$

where k is the angular wavenumber. For the surface power variation due to roughness to not exceed 2 dB, h_{rms} should be less than 0.35 m in the region around aquifers, i.e., the reflectometry regime in Fig. 1(b). In this regime, the surface is flat enough to directly map higher levels of surface echo to the dielectric contrast caused by a shallow water table.

However, by accurately modeling roughness response, it is possible to infer the dielectric contrast even where $h_{rms} > 0.35$ m. In this case, the detectability of shallow aquifers would depend on the uncertainty in the predicted roughness response ($\Delta P/P$) caused by an uncertainty Δh_{rms} in the knowledge of the terrain elevation variations h_{rms}, given by

$$\Delta P/P = 8k^2 h_{rms} \Delta h_{rms} \qquad (2)$$

and shown in Fig. 1(b). By analyzing this graph, we find that in the absence of other forward model errors, h_{rms} must be known to better than 0.3 m at an h_{rms} of 0.5 m (smooth regime) to predict the power variation due to roughness within 3-dB uncertainty.

Finally, several techniques exist to simultaneously retrieve roughness and dielectric properties by analyzing the surface echo waveform and amplitude, with the support of digital elevation models, rough surface scattering models, clutter simulations, or by fitting statistical distributions to echo amplitude samples (e.g., [14], [15]). Joint inversion techniques may be necessary if the conditions above are not met, i.e., if the roughness in the region of interest is too large or the knowledge of the roughness is too uncertain.

III. RESULTS

This section describes the simulation of the radar response of different aquifer models. All the simulations consider the sounding radar parameters described in Table I with both the omnidirectional antenna (MONO) and the distributed array (DIST) configurations for comparison. For DIST models,
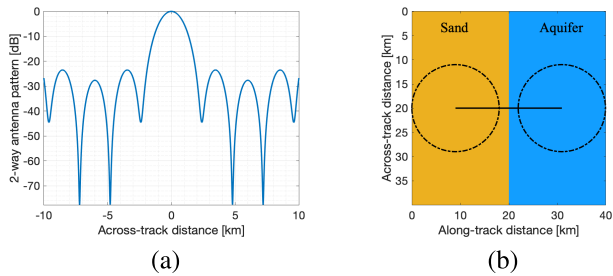
Fig. 2. (a) Two-way cross-track antenna pattern of the distributed architecture in terms of power in dB. In this configuration, all the satellites are assumed to be transmitting and receiving. (b) Subsurface dielectric setting of the model used for studying the transition from the absence to the presence of the shallow aquifer. The flat subsurface is partitioned into two halves: the left half representing dry sand $\epsilon' = 4$, $\epsilon'' = 0.08$, the right half representing aquifer $\epsilon' = 14$. The black line is the radar track, while the circles represent the simulation footprint at the end points of the track.

TABLE I
RADAR SOUNDER INSTRUMENT PARAMETERS COMMON TO BOTH MONO AND DIST CONFIGURATIONS

Parameters	Values
Central frequency	45 MHz
Bandwidth	8 MHz
Peak radiated power	100 W
Spacecraft altitude	450 km
Sampling frequency	12 MHz
Pulse repetition frequency (PRF)	300 Hz

we consider five mini-satellites in flying formation oriented orthogonal to the direction of flight operating in full phased array mode, i.e., all the satellites are transmitting and receiving. The spacing between two adjacent satellites is 250 m. The beam pattern resulting from this configuration is shown in Fig. 2(a).

A. Sensitivity Analysis: Flat Surface Models

First, we analyze the sensitivity of the instrument to the presence of the shallow aquifer at different depths below the surface, assuming the ideal case of no surface or subsurface roughness. For these experiments, the model comprises two flat layers of which the surface is composed of dry sand ($\epsilon' = 4$, $\epsilon'' = 0.08$), while for the subsurface, the below cases are considered.

1) Composed of dry sand (i.e., subsurface same as the surface).
2) Composed purely of saturated sand associated with the aquifer ($\epsilon' = 14$). The radar footprint surface projected trajectory is ≈7 km long.
3) Half of the width comprises dry sand, and the other half comprises saturated sand associated with the aquifer ($\epsilon' = 14$). The radar footprint surface projected trajectory of length ≈22 km is defined as symmetrically transiting from dry to saturated sand [see Fig. 2(b)].

In the second and third cases, the depth d of the subsurface layer is varied as $d = \{5, 10, 15, 20\}$ m. The simulation footprint is circular with a radius of 9 km.
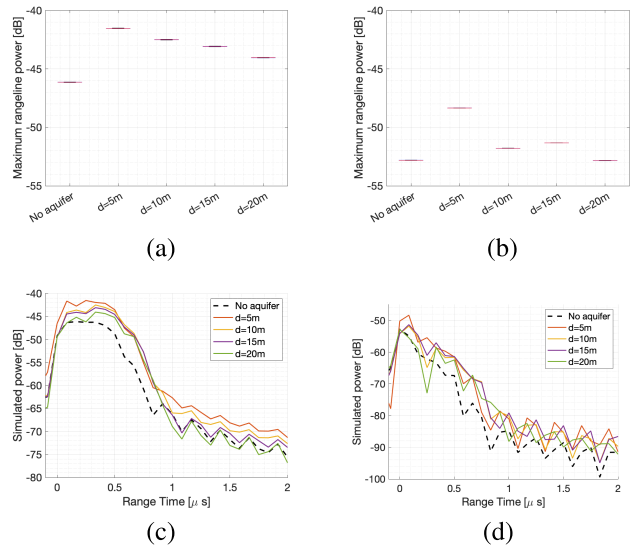

Fig. 3. Sensitivity analysis for the flat models in which the subsurface (where present) is composed purely of saturated sand. Boxplots showing variations in maximum rangeline power across the simulated track for different depths d of the aquifer for (a) MONO and (b) DIST configurations. Plot of the central rangeline in the simulated radargrams of (c) MONO and (d) DIST configurations.
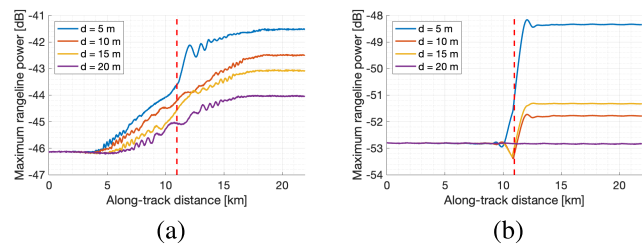

Fig. 4. Plot of maximum rangeline power along the radar track traversing from dry sand to flat aquifer half-space [see Fig. 2(b)] placed at different depths for (a) MONO and (b) DIST configurations. The red dashed line indicates the nadir position of the start of the aquifer half.

Fig. 3 shows the results of the first and second cases in terms of the variations in the maximum rangeline power (Fig. 3(a) MONO and (b) DIST) and the central rangeline (Fig. 3(c) MONO and (d) DIST) of the range-compressed radargrams. Note that the central rangelines show only a single peak since the depth (maximum 20 m) to the aquifer is comparable to the range resolution of the instrument (about 10 m in sand at the 8-MHz bandwidth). Thus, the maximum power combines the contribution from the surface and the subsurface. Fig. 4 shows the results of the third case, i.e., the half-space aquifer models, in terms of the maximum rangeline power along the track transiting from dry to saturated sand.

With both the MONO and DIST configurations, the radar has a sensitivity of about 4–5 dB to the presence of the shallowest aquifer ($d = 5$ m). At greater depths (e.g., $d = 20$ m), it may not be possible to detect the aquifer by only analyzing the maximum rangeline power, especially with the distributed architecture. However, the rangeline plots [see Fig. 3(c) and (d)] show that the deeper aquifers may produce a delayed response, without presenting a distinguishable peak in the rangelines. The delayed response may be detectable using
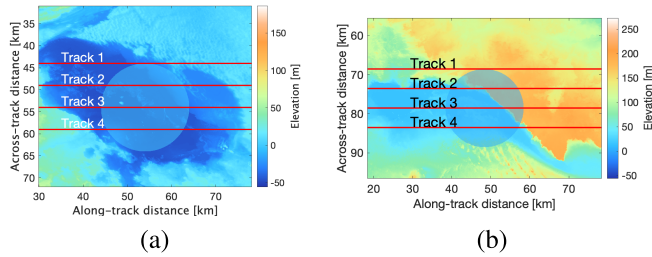
Fig. 5. Aquifer models (a) Model-A (centered at 29.85°N, 19.7°E) and (b) Model-B (centered at 29.3°N, 19.22°E) developed using Copernicus DEMs of the two study areas. The circle represents the location of the flat aquifer modeled in the subsurface. The red lines denote the four radar tracks traversing the aquifers.

standard radar sounder data processing techniques. With the omnidirectional antenna, we see a sequential decrease in the surface peak power with increasing depth of the aquifer [see Figs. 3(a) and (c) and 4(a)]. Whereas in the distributed case [see Fig. 3(d)], the rangelines show this ordered progression close to a delay time of 0.5 μs. The rangeline plot also helps explain why $d = 20$ m does not show any difference in terms of maximum rangeline power in Figs. 3(b) and 4(b).

B. Realistic Aquifer Simulations

Based on the previous experiments, we considered realistic surface roughness conditions to understand their effects on the detectability of the aquifers. For this purpose, we modeled a circular aquifer of radius 10 km with a flat water table located 5 m below the deepest point within the circle shown in Fig. 5(a) and (b).

Model-A represents the area near the Ma'tan al Jafr well, while Model-B is defined around the Marada oasis. We have used 30-m resolution Copernicus GLO 30 digital surface models acquired by TanDEM-X [16] to build our topographic models. In terms of surface roughness, Model-A has lower h_{rms} that is expected to favor the identification of the aquifer, while Model-B is a challenging scenario with higher roughness. Outside and above the circular aquifer, the models consider the presence of dry sand with dielectric permittivity $4 + i0.08$. The aquifer itself is modeled with a real permittivity of 20.

Note that the depth of the aquifer varies from 5 to 70 m (Model-A) and from 5 to 170 m (Model-B) due to spatial variations in surface elevation. To confirm the presence of an aquifer, it is worthwhile to look for its evidence in multiple parallel radar tracks. Here, we consider four parallel tracks traversing the aquifer and spaced 5 km apart. The radar simulation footprint is set to 13 km to account for clutter that can potentially interfere with the aquifer response. To clearly distinguish the echo from the aquifer from the one from surface clutter, we simulate two scenarios for each track: 1) the presence of the aquifer as described in Fig. 5 (also referred to as "radargram" or "aquifer" in this letter) and 2) the absence of the aquifer (also referred to as "cluttergram" or "no aquifer" in this letter). The ratio of the subsurface response to the clutter response is used as an estimate for the expected signal-to-clutter ratio (SCR).

We present the radargrams and cluttergrams for Track 3 (i.e., the track passing through the center of the circular aquifer).
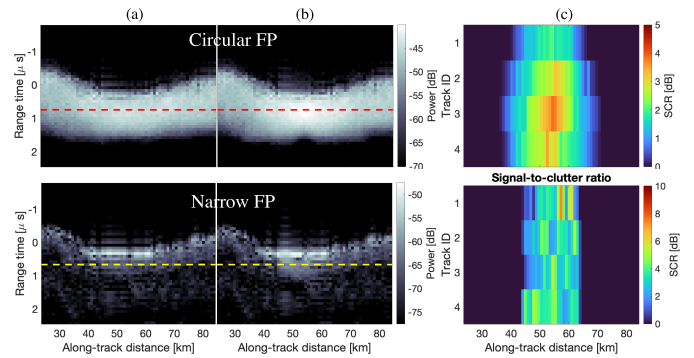

Fig. 6. Simulated Model-A radar response with the MONO configuration for (a) no aquifer, (b) aquifer present in the subsurface cases, and (c) corresponding SCR. All the radargrams correspond to Track 3 in Fig 5(a). The top results are obtained using a circular footprint of 13-km radius, while the bottom ones are obtained with narrow 1.5 × 60 km rectangular footprints to represent the effect of focusing. SCR is evaluated at the range time indicated by red and yellow dashed lines in the radargrams.
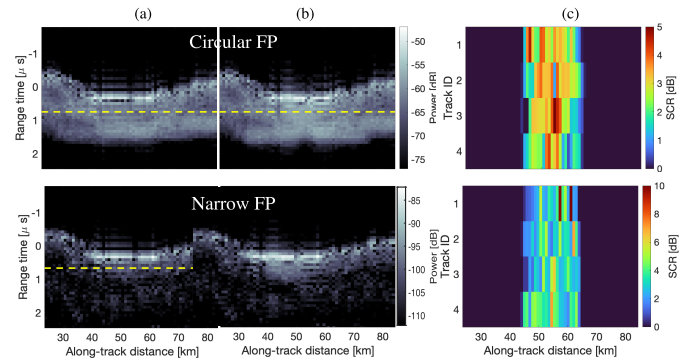

Fig. 7. Simulated Model-A radar response of Track 3 with the DIST configuration for (a) no aquifer, (b) aquifer present in the subsurface cases, and (c) corresponding SCR evaluated at the range time indicated by yellow-dashed lines in the radargrams.
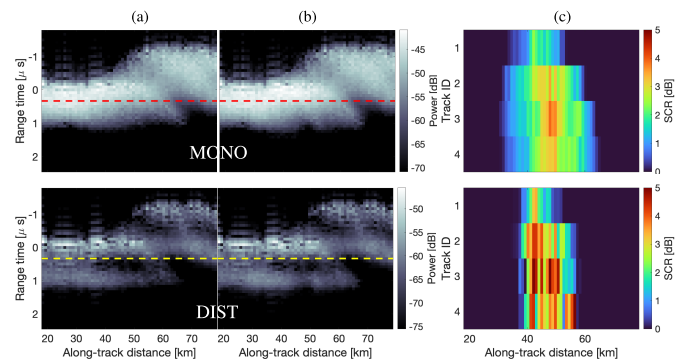

Fig. 8. Simulated Model-B radar response for (a) no aquifer, (b) aquifer present in the subsurface cases, and (c) corresponding SCR evaluated at the range time indicated by red and yellow-dashed lines in the radargrams. All the radargrams have been obtained considering a circular footprint of radius 13 km and correspond to Track 3 in Fig 5(b). The top results correspond to the MONO configuration, while the bottom ones correspond to the DIST configuration.

However, in the supplementary information, we provide video files showing the variation in echo power at every time delay as the signal propagates through the medium. Figs. 6–8 show the simulated aquifer radargrams, cluttergrams, and SCR for different satellite configurations and the two aquifer models. The SCR plot is a four-row matrix in which each row corresponds

to Tracks 1–4 (from top to bottom). The SCR values in each track are computed at the delay time indicated by red-dashed lines in the radargrams. Since Model-A represents a more likely aquifer scenario, we analyzed it in further detail by considering the effect of SAR focusing in the simulation process. Note that it was not possible to apply the actual SAR-focused processing to the data since we reduced the PRF to 8 Hz (≈1 pulse per kilometer) to optimize the computational time. Thus, focusing was approximated by considering narrow rectangular footprints of across-track width 1.5 km (approximately equal to the Fresnel zone radius) and length 60 km (to collect maximum off-nadir clutter contribution).

In all the cases, the central rangelines of the radargrams (where the aquifer is present at nadir) show a stronger echo than the clutter response. This is further evident in the SCR plots, which indicate about 5 dB or higher SCR due to the presence of the aquifer. Compared with the omnidirectional antenna, the distributed architecture further improves the SCR metric, as expected. Finally, Model-B, which represents a relatively more challenging scenario for aquifer detectability, also shows a high value of SCR, especially using the distributed configuration.

IV. CONCLUSION

In this letter, we have analyzed the sensitivity of an Earth-orbiting 45-MHz radar sounder to assess the presence of shallow aquifers in the first 10 m by reflectometry in arid areas. Two different transceiver configurations were considered—an omnidirectional and a distributed array of five orbiting mini-satellite formation, both of which were found to be sensitive to the aquifer presence, although the distributed configuration performed better in terms of clutter reduction, as expected. The use of a ray tracing simulator in this study ensures that the cluttergrams are precisely matched with the subsurface radargrams. In reality, the inability to exactly represent the acquisition scenario translates to inaccuracies in the clutter simulations. The results obtained in our investigation show that the surface cluttergram requires an accuracy of 2–3 dB, such that when we compare the cluttergram to the measured radargram, the difference in power of 5 dB can be interpreted by the presence of an aquifer.

Given the availability of high-resolution DEMs for terrestrial arid zones, the accuracy of the clutter simulations will mainly depend on the ray tracing simulator's capabilities. In this initial investigation, we have considered a facet-based multilayered simulator. However, for future more in-depth investigation of this work, we will use advanced numerical simulators such as the dictionary-based integrated approach capable of accurately modeling small-scale roughness response (e.g., [17]). Alternatively, the surface power needs to be accurately calibrated using tie points before and after the acquisition over the arid aquifer region, possibly using in situ calibration and validation. Future extensions of this work will consider these factors to develop techniques that

allow unambiguous detection of the aquifers from spaceborne radargrams.

REFERENCES

[1] L. Bruzzone, F. Bovolo, L. Carrer, E. Donini, and S. Thakur, "STRA-TUS: A new mission concept for monitoring the subsurface of polar and arid regions," in *Proc. IEEE Int. Geosci. Remote Sens. Symp.*, Jul. 2021, pp. 661–664.

[2] G. Gennarelli et al., "A low frequency airborne GPR system for wide area geophysical surveys: The case study of Morocco desert," *Remote Sens. Environ.*, vol. 233, Nov. 2019, Art. no. 111409.

[3] E. Heggy et al., "Airborne sounding radar for desert subsurface exploration of aquifers: Desert-SEA: Mission concept study [space agencies]," *IEEE Geosci. Remote Sens. Mag.*, vol. 12, no. 1, pp. 162–185, Mar. 2024.

[4] L. Carrer, C. Gerekos, F. Bovolo, and L. Bruzzone, "Distributed radar sounder: A novel concept for subsurface investigations using sensors in formation flight," *IEEE Trans. Geosci. Remote Sens.*, vol. 57, no. 12, pp. 9791–9809, Dec. 2019.

[5] E. Heggy, "Exploring deserts response to climate change from the Orbiting Arid Subsurface and Ice Sheet Sounder (OASIS)," in *Proc. IEEE Int. Geosci. Remote Sens. Symp. (IGARSS)*, Jul. 2021, pp. 655–656.

[6] A. Freeman, X. Pi, and E. Heggy, "Radar sounding through the Earth's ionosphere at 45 MHz," *IEEE Trans. Geosci. Remote Sens.*, vol. 55, no. 10, pp. 5833–5842, Oct. 2017.

[7] S. Thakur, E. Donini, F. Bovolo, and L. Bruzzone, "An approach to the assessment of detectability of subsurface targets in polar ice from satellite radar sounders," *IEEE Trans. Geosci. Remote Sens.*, vol. 60, pp. 1–21, 2021.

[8] R. Culberg and D. M. Schroeder, "Firn clutter constraints on the design and performance of orbital radar ice sounders," *IEEE Trans. Geosci. Remote Sens.*, vol. 58, no. 9, pp. 6344–6361, Sep. 2020.

[9] C. Gerekos, A. Tamponi, L. Carrer, D. Castelletti, M. Santoni, and L. Bruzzone, "A coherent multilayer simulator of radargrams acquired by radar sounder instruments," *IEEE Trans. Geosci. Remote Sens.*, vol. 56, no. 12, pp. 7388–7404, Dec. 2018.

[10] G. Scabbia and E. Heggy, "Quantifying subsurface propagation losses for VHF radar sounding waves in hyper-arid terrains," in *Proc. IEEE Int. Geosci. Remote Sens. Symp.*, Jul. 2018, pp. 6800–6803.

[11] E. Heggy et al., "Probing shallow aquifers in hyperarid dune fields using VHF sounding radar," *IEEE Trans. Geosci. Remote Sens.*, vol. 61, 2023, Art. no. 4505822.

[12] J. C. Fontes, M. Yousfi, and G. B. Allison, "Estimation of long-term, diffuse groundwater discharge in the northern Sahara using stable isotope profiles in soil water," *J. Hydrol.*, vol. 86, nos. 3–4, pp. 315–327, Oct. 1986.

[13] P. Paillou et al., "Performances of ground penetrating radars in arid volcanic regions: Consequences for Mars subsurface exploration," *Geophys. Res. Lett.*, vol. 28, no. 5, pp. 911–914, Mar. 2001.

[14] C. Grima et al., "Investigating the Martian surface at decametric scale: Population, distribution, and dimension of heterogeneity from radar statistics," *Planet. Sci. J.*, vol. 3, no. 10, p. 236, Oct. 2022.

[15] L. Carrer, F. Zancanella, and L. Bruzzone, "Mars surface imaging by exploiting off-nadir radar sounding data," *IEEE Trans. Geosci. Remote Sens.*, vol. 59, no. 4, pp. 2951–2961, Apr. 2021.

[16] *Copernicus Dem*, Eur. Space Agency, 2022, doi: 10.5270/ESA-c5d3d65.

[17] E. Sbalchiero, M. Cortellazzi, S. Thakur, and L. Bruzzone, "A dictionary-based integrated simulation approach to model large- and small-scale coherent surface scattering phenomena in radar sounder data," *IEEE Trans. Geosci. Remote Sens.*, vol. 61, 2023, Art. no. 4600819.